Research Article

77

INDONESIAN SCHOLAR SOCIETY

Indones. J. Chem. Stud.
2025, 4(2), 77–86
Available online at journal.solusiriset.com
e-ISSN: 2830-7658; p-ISSN: 2830-778X

Indonesian Journal of Chemical Studies

Temperature Combustion Profiles of KNO_3, $CsNO_3$, and $NaNO_3$-Based Energetic Materials at Atmospheric Pressure

Nguyen Duy Tuan[1], Denisuyk A. P.[2], Hoang Trung Huu[1], Sizov V.A.[2], Doan Minh Khai [1]*

[1]*Le Quy Don Technical University, 236 Hoang Quoc Viet, Bac Tu Liem, Ha Noi, Viet Nam*

[2]*Mendeleev University of Chemical Technology of Russia, 9 Miusskaya Square, 125047 Moscow, Russia*

Received: 23 May 2025; Revised: 27 Aug 2025; Accepted: 23 Sep 2025;
Published online: 30 Oct 2025; Published regularly: 31 Dec 2025

Abstract— This study investigated the thermal properties of energetic materials composed of alkaline metal nitrates, specifically KNO_3, $CsNO_3$, and $NaNO_3$, at atmospheric pressure. This study primarily evaluated the burning surface temperature and characterized the heat release behavior of the studied compositions during combustion. To determine the thermal output, temperature profiles were obtained using thermocouple wires on the combustion surface. Given the heterogeneous structure of these formulations and the reactivity of alkali metals during combustion, finding a consistent temperature signatures presented an analytical challenge. All the tested samples exhibited very high surface combustion temperatures. The KNO_3-based sample exhibited a higher maximum heat-flow density than the $NaNO_3$-based formulation. Variations in the temperature profiles resulted from the differences in composition structure and combustion reactivity. This study showed the effect of nitrate type on the thermal performance of energetic materials. These results clarified the influence of nitrate identity on heat transfer and combustion efficiency in nitrate-based pyrotechnic formulations, and may inform the design of thermally stable, high-performance propellants and thermal generator formulations.

Keywords— *Combustion; $CsNO_3$-based sample; KNO_3-based sample; $NaNO_3$-based sample; Temperature profile*

1. INTRODUCTION

In the realm of high-energy material production, inorganic nitrates are frequently employed. Current research focuses on the combustion mechanisms of these materials. Alkali metal nitrates possess very high melting and decomposition temperatures. Various researchers have investigated the differential thermal analysis and thermogravimetric analysis of KNO_3 [1-7]. Research results from [4] show that during the heating process of KNO_3, an endothermic peak appears at 403 K, signifying a transition in the crystal structure from rhombic to trigonal. Another endothermic peak is observed at 610 K, which corresponds to the melting point of KNO_3. Notably, KNO_3 melts without undergoing decomposition or gasification, maintaining stability in its molten state over a broad temperature range from its melting point to 773 K. The decomposition of KNO_3 occurs in two stages at temperatures of 773-1043 K and 1043-1273 K. A weight loss of KNO_3 is 72.0±1.2% at temperatures from 773 K to 1043 K and 14.0±1.0% from 1043 to 1273 K. According to [7], in an argon atmosphere, rapid weight loss of KNO_3 begins at 848 K, with the starting peak of endothermic degradation observed at 863 K. Under an air atmosphere, rapid weight loss of KNO_3 starts at 863 K, with the starting peak of endothermic degradation observed at 868 K. In oxygen, rapid weight loss begins at 873 K, with the starting peak of endothermic degradation observed at 863 K. In the nitrogen atmosphere, the decomposition of KNO_3 occurs at 894.3 K, resulting in a mass reduction of approximately 65% [1, 3].

According to [5, 7-9], $NaNO_3$ exhibits a rapid weight loss starting at 841 K in an argon atmosphere, with the initiation of endothermic degradation observed at 838 K. Under an air atmosphere, the rapid weight loss of $NaNO_3$ initiates at 848 K, with the starting peak of endothermic degradation noted at 845 K. In an oxygen atmosphere, the rapid weight loss of this nitrate begins at 863 K, with the starting peak of endothermic degradation observed at 821 K. Additionally, the decomposition of $NaNO_3$ in nitrogen atmosphere occurs at 816.7 K, with a mass loss of approximately 70% [3, 10]. As [5, 6, 9], the decomposition of $CsNO_3$ occurs at high temperatures (above 673 K).

***Corresponding author**.
Email address: khaihv@lqdtu.edu.vn
DOI: 10.55749/ijcs.v4i2.74

The combustion mechanism for pyrotechnic mixtures of "nitrate/metal" has been extensively studied. Consider the combustion mechanism of a binary mixture of Mg and $NaNO_3$ as an example [11-16]. These components differ in temperature characteristics; for instance, $NaNO_3$ melts at a temperature of ~581K and decomposes at 870K, unlike Mg, which melts and boils at 932K and 1380K, respectively. Mg remains condensed, whereas $NaNO_3$ has already decomposed. At the combustion surface of the firework, nitrite and oxygen are detected, indicating decomposition of the nitrate. As a result, the gaseous flow of oxygen carries away $NaNO_2$ and Mg droplets, which ignite near the surface of the mixture, transitioning into the diffusion regions of combustion. The combustion of Mg particles and their products releases a significant amount of heat, which increases the temperature. This, in turn, generates conductive and radiative heat fluxes directed toward the combustion surface of the system. Simultaneously, the combustion of Mg leads to further heating and intense decomposition of $NaNO_2$. Additionally, heat release occurs due to the retention of some Mg particles on the system surface. The combination of conductive and radiative fluxes with heat release results in a specific compensation for the heat required to heat the mixture to the temperatures of $NaNO_3$ decomposition and Mg melting. The combustion of Mg in the atmosphere of gaseous oxidizer decomposition products releases most of the heat, and the heat input to the condensed phase plays a less significant role. The combustion of the $Mg/NaNO_3$ mixture is highly dependent on the condensed phase heat and the reaction zone temperature [11].

A decrease in the Mg content increases the agglomeration of metal particles, decreases the temperature of the condensed phase, and reduces the extent of the reaction zone, thereby declining the combustion rate. A change in the initial temperature of the mixture can lead to a change in the degree of metal agglomeration and the amount of heat released by the condensed phase, contributing to the high-temperature sensitivity of the combustion rate of the system. The combustion of pyrotechnic compositions based on inorganic nitrates with the addition of Mg can occur in various zones: the heating zone, the zone of overall exothermic reactions in the c-phase, at the gas-c-phase interface, and the zone of exothermic reactions in the flame. The oxidizer and metallic fuel particles do not burn at the same temperature.

The combustion behavior of materials based on various inorganic nitrates and phenol-formaldehyde resin (PFR) plasticized by dibutyl phthalate (DBP) has been studied [17-19]. However, the combustion mechanism of the samples has not been investigated. This work aims to examine the mechanism of combustion of KNO_3, $CsNO_3$, and $NaNO_3$-based samples at atmospheric pressure.

Denisyuk A.P. et al investigated the thermal decomposition characteristics of individual PFR under non-isothermal conditions. Their results revealed that the majority decomposition of PFR occurred within the temperature range of 650-850 K. However, the mixtures of KNO_3 containing 14% PFR exhibit a weight loss at around 550 K, continuing up to 660 K [20]. This behaviour indicates that the interaction between nitrate and PFR with a plasticizer significantly lowers the thermal stability relative to the pure nitrate and PFR components.

2. EXPERIMENTAL SECTION

2.1. Materials

Alkali metal nitrates (KNO_3, $CsNO_3$, and $NaNO_3$; 99% purity) were employed in this study. The PFR was plasticized with DBP at a PFR to DBP mass ratio of 3:2. To improve the physico-mechanical and technological characteristics, 1.5% wt% teflon and 0.5% wt% calcium stearate were introduced into the samples. The samples were prepared with an excess oxidizer coefficient (α) of 0.72 to investigate the combustion mechanism. The excess oxidizer coefficient represents the ratio between the actual amount of oxidizer and the stoichiometric requirement for complete combustion. Based on their combustion performance at atmospheric pressure, the samples were categorized as follows [17-19]: (1) fast-burning compositions, based on KNO_3 and $CsNO_3$, exhibiting buring rates - r_b(0.1) of 5.2 and 4.6 mm/s, respectively; (2) slow-burning compositions, based on $NaNO_3$, with a burning rate r_b(0.1) of 1.5 mm/s.

2.2. Procedure

The samples were prepared following the procedure described in Refs. [17-19]. The oxidizing agents were preliminarily dried and mixed with PFR and technological additives, after which the plasticizer was incorporated. The resulting mixture was homogenized until a uniform mass with a wet sand-like consistency was obtained. The mixture was then rolled using a 0.6 mm roll gap and pressed into cylindrical charges with a diameter of 7 mm for the determination of the burning rate and temperature profiles. The burning rate was measured according to the method reported in Refs. [17-20], with an experimental uncertainty of ±2%.

Thermogravimetric analysis (TGA) was performed using a thermogravimetric analyzer to monitor mass changes as a function of temperature. The samples were placed in a special crucible and analyzed under a nitrogen atmosphere. Measurements were conducted at a heating rate of 20K/min over a temperature range of 0 - 1273 K.

The combustion temperature and temperature profiles of the samples were measured using tungsten rhenium (W-Re) thermocouple wire with a thickness of 3-5 μm. The thermocouple wire complied with the GOST 8.585-2021 standard and met the technical conditions of

SU0.021.142 TU, confirming its suitability for high-temperature measurements. Each sample, compressed with thermocouple wire, was placed in a constant-pressure combustion chamber and burned under a nitrogen atmosphere to prevent the interactions between combustion products and atmospheric oxygen.

3. RESULT AND DISCUSSION

3.1. TGA Results of The Samples

The results of TGA of the samples with a heating rate of 20 K/min are shown on **Fig. 1.** The slow-burning $NaNO_3$-based composition (r_b(0.1) = 1.5 mm/s) exhibited a similar flash temperature (T_f ~653 K) and mass loss 28,8-32.7% to that of the KNO_3-based formulation (r_b(0.1) = 5.2 mm/s). In contrast, the $CsNO_3$-based composition (r_b(0.1) = 4.6 mm/s) displayed a higher flash temperature (T_f = 683 K), and a greater mass loss (Δm =46.8%).

It is assumed that during the combustion of the studied compositions, consisting of nitrates and the decomposition products of PFR (mainly condensed ones), their intensive interaction occurs without the decomposition of these nitrates into molecular oxygen. The primary solid products formed during the decomposition of PFR include [21]: (a) Amorphous carbon (char) – the dominant solid residue, generated through extensive cross-linking and carbonization processes during pyrolysis; (b) Carbonaceous structures with variable graphitization – depending on the temperature, partial ordering of carbon layers may occur at higher pyrolysis stages; and (c) Mineral residues (trace inorganic content) – usually present in minor quantities, originating from catalysts or additives used in resin synthesis.

$$PFR \xrightarrow{\Delta} C_{amor.} + phenol.derivatives + CO, CO_2, CH_4, H_2, etc.$$

At higher temperatures, the residual oxidizers decompose, releasing molecular oxygen that subsequently reacts with the gaseous decomposition products of PFR and the plasticizer (or its decomposition products) within the flame zone above the burning surface [20]. The reactions can be represented as follows (Equation 1 – 6).

$$3C + 2MNO_3 \rightarrow M_2CO_3 + N_2 + CO_2 + CO \quad (1)$$

$$5C + 4MNO_3 \rightarrow 2M_2CO_3 + 2N_2 + 3CO_2 \quad (2)$$

$$5C + 4MNO_3 \rightarrow 2M_2O + 2N_2 + 3CO_2 \quad (3)$$

$$M_2O + CO_2 \rightarrow M_2CO_3 \quad (4)$$

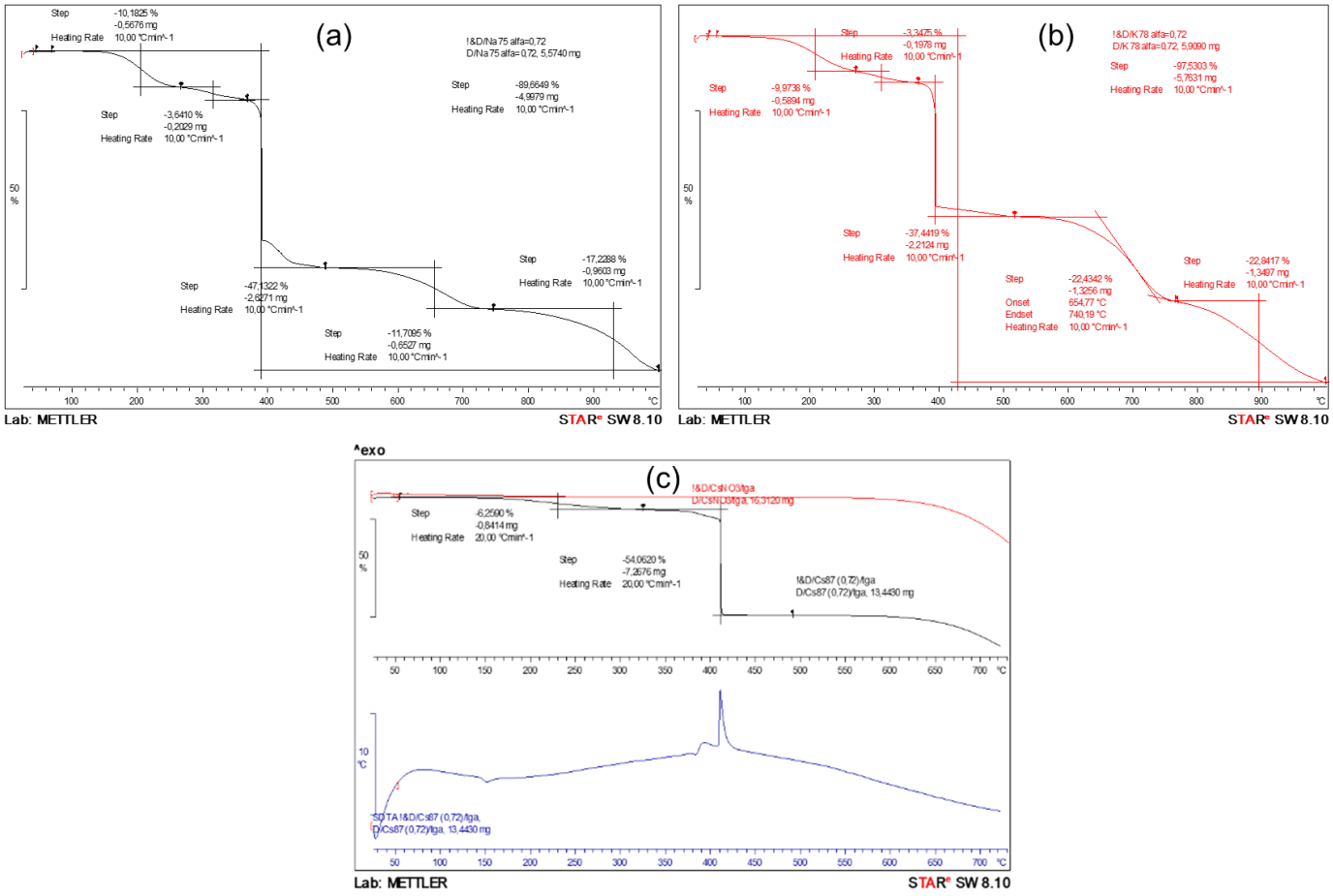

Fig. 1. Thermogravimetric analysis (TGA) of samples based on alkali metal nitrates: (a) KNO_3-based sample; (b) $NaNO_3$-based sample; (c) $CsNO_3$-based sample

$$2MNO_3 \rightarrow 2MNO_{2(l.)} + O_2 \quad (5)$$

$$2MNO_{2(l.)} \rightarrow 1M_2O + 2NO + 1/2O_2 \quad (6)$$

With: M = K, Cs, Na. Consequently, the solid combustion ends up mainly as K_2CO_3 (and sometimes K_2O), with gaseous products including N_2, CO_2, and CO.

3.2. Temperature Profile Parameters in The Combustion Wave

For all the tested samples, the temperature-time relationship during combustion is documented on the oscillograms (**Fig. 2**). Once the burning rate is determined, it becomes feasible to transform the graph from a temperature-time dependence to a temperature-distance (T_x) dependence.

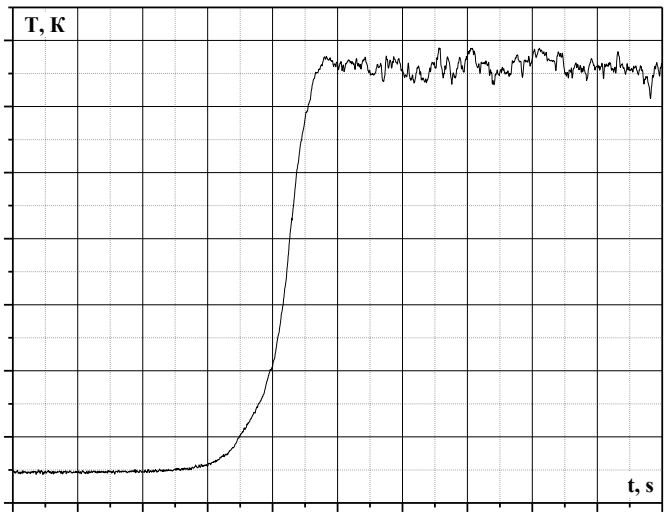

Fig. 2. The typical oscillogram of the temperature combustion of sample combustion over time

During the experiments, the temperature-time (T-t) relationship of the samples was recorded as an oscillogram. Using the known burning rate, this dependence was subsequently converted into a temperature-distance (T-x) profile. Variations in the heterogeneous structure of the compositions, combined with the high chemical aggressiveness of alkali-containing combustion products toward thermocouple materials, produced oscillatory and pulsating temperature traces. These effects complicate the identification of characteristic thermal points (**Fig. 3**) [18, 22, 23].

Additional challenges arise in selecting the combustion surface temperature during the T(x) curve processing. In some oscillograms, a temperature drop was observed immediately after the temperature exceeded the melting point, attributed to the impact of dispersed droplets from the condensed (c) phase-molten particles with a boiling point lower than the temperature zone where the thermocouples were located. In many of the studied samples, the thin thermocouples are almost broken at a small distance from the combustion surface.

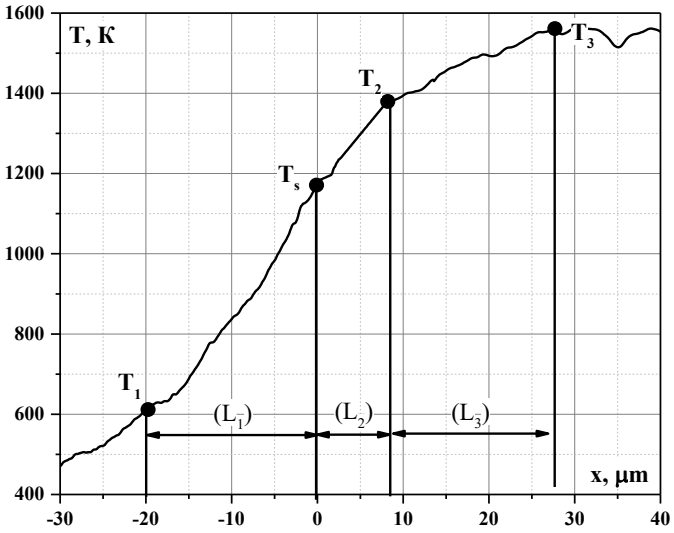

Fig. 3. The typical oscillogram of the temperature profile in the combustion wave of the samples

The characteristic inflection point (x=0) is considered as the surface temperature, marking the transition of the thermocouple junction from the condensed (c) phase to the gaseous (g) phase. In the oscillograms, L_1 represents the width, encompassing the heated layer and reaction layer of the c-phase, where the temperature decreases by e times (Equation 7).

$$\frac{T_s - T_o}{T_1 - T} = e \rightarrow T_1 = \frac{T_s - T_o}{e} + T_o \quad (7)$$

According to L_1, the coefficient of thermal diffusivity is determined: $\chi = L_1.r_b$; L_2 represents the width of the combustion zone, where exothermic reactions between the combustible decomposition products of the resin and NO or oxygen in the g-phase are likely completed, and small soot particles burn out with an endothermic effect, leading to a temperature transition from T_s to T_2 (Equation 8).

$$\varphi = \frac{dT}{dx} = \frac{T_2 - T_s}{L_2} \quad (8)$$

Symbol Φ represent the temperature gradient over the combustion surface ranges from T_s to T_2. The gradient ϕ is utilized to calculate the heat balance of the c-phase; L_3 denotes the distance, at which big soot particles burn out, resultingin a temperature increase from T_2 to the maximum temperature T_3.

The obtained results are shown in Tables 1-3. The measured burning rate was 5.2 mm/s for the KNO_3-based sample while the theoretical combustion temperature (T_t) was 1516 K [18] (**Fig. 4**). The surface temperature T_s of the sample at atmospheric pressure varied within a range of 1177-1327 K (**Fig. 5, Table 1**). The width of the heated and reaction layers in the c-phase ranged from 10 to 24 μm, with the temperature gradient over the combustion surface estimated between 1.17 x 10^4 and 2.58 x 10^4 K/mm.

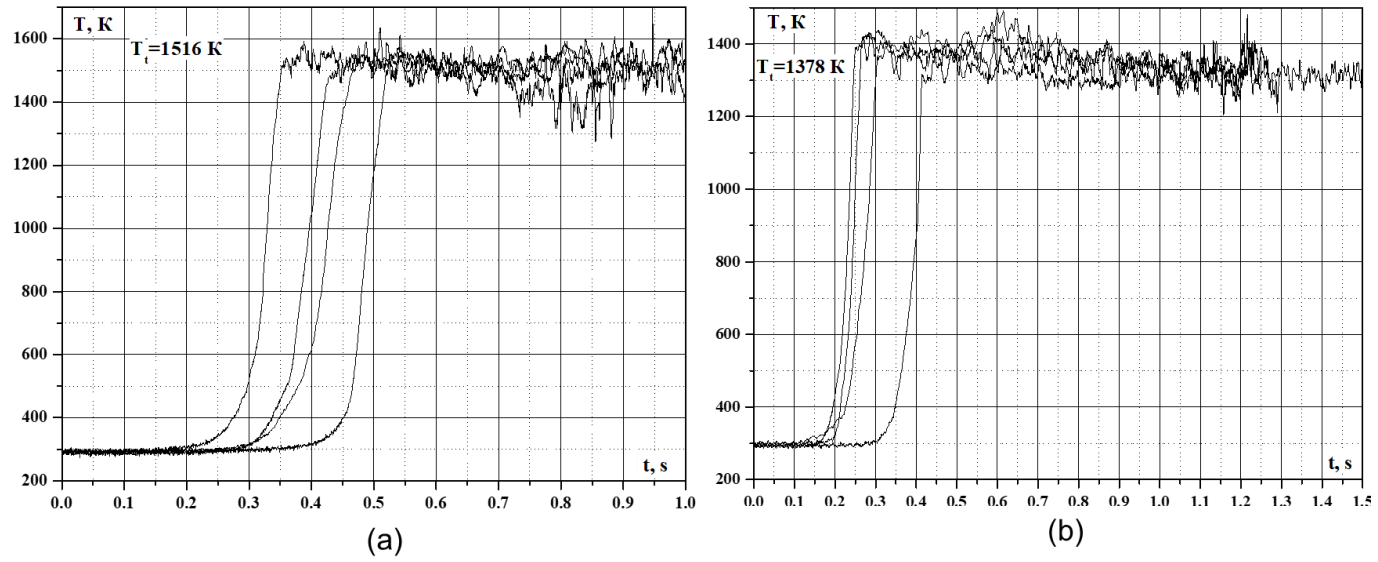

Fig. 4. Experimental combustion temperature of samples based on KNO_3 (a) and $CsNO_3$ (b) at atmospheric pressure

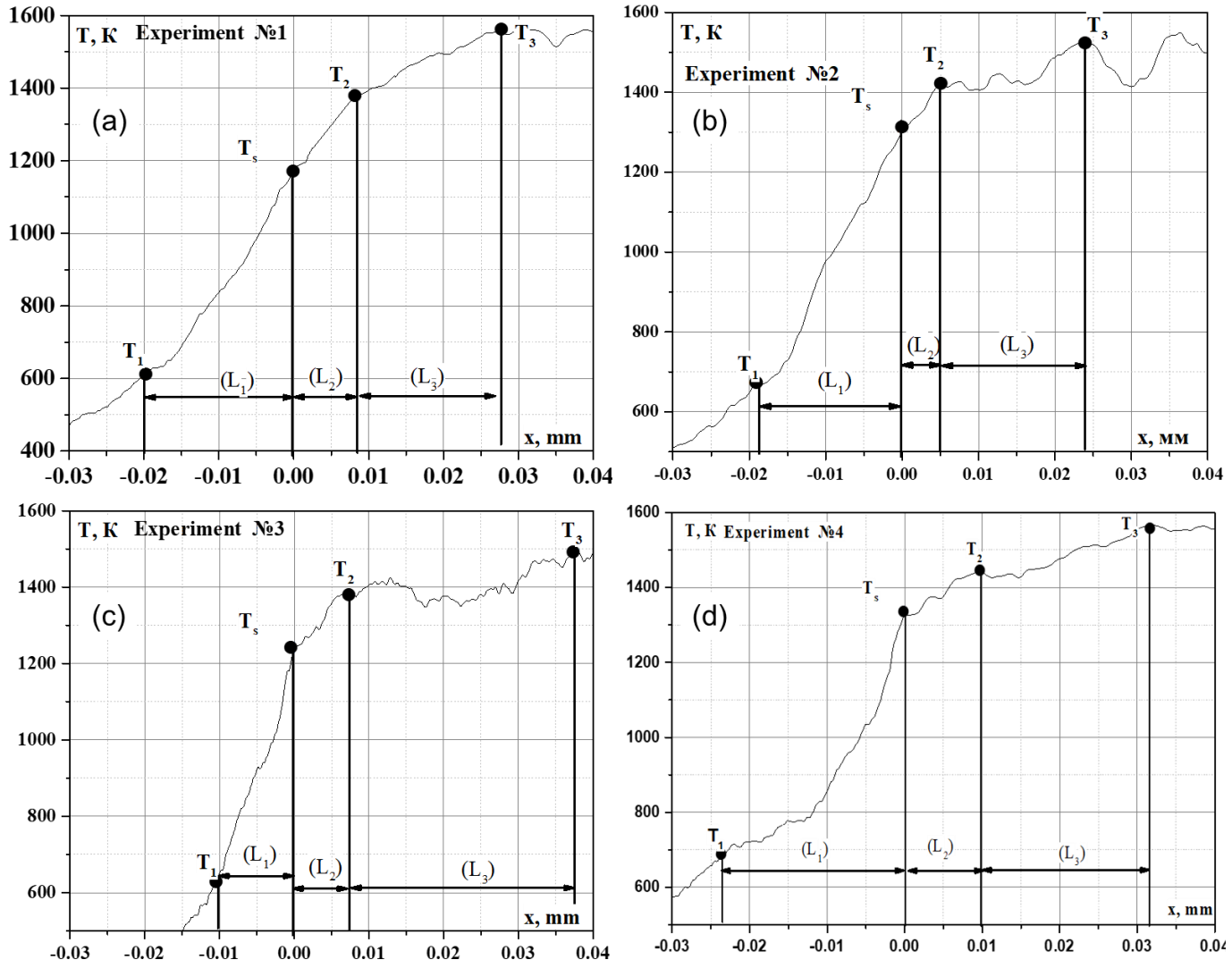

Fig. 5. The typical oscillogram of the temperature profiles in the combustion wave of the KNO_3-based sample at atmospheric pressure

The oscillograms of the $CsNO_3$-based sample exhibited distinct combustion regions. The combustion characteristics of the sample are outlined as follows: T_s ranging from 1233 to 1288 K (**Table 1, Fig. 6**); the lengths

of the widths L_1, L_2, L_3 are within the range of 31 to 55, 8 to 13, and 54 to 71 µm, respectively. The temperature gradient ϕ, varies between approximately 0.59×10^4 and 0.97×10^4 K/mm. The coefficient of thermal diffusivity for the sample lies in the range of 0.14 to 0.25 mm^2/s.

Table 1. Temperature parameters in the combustion wave of the alkaline metal nitrate sample

Alkaline Metal Nitrates Experiment	T_1 (K)	L_1 (µm)	χ (mm^2/s)	T_s (K)	ϕ (10^{-4} K/mm)	T_2 (K)	L_2 (µm)	T_3 (K)	L_3 (µm)
KNO_3 (1)	673	24	0.13	1327	1.17	1444	10	1560	22
KNO_3 (2)	668	18	0.09	1309	2.06	1412	5	1522	19
KNO_3 (3)	644	10	0.05	1245	2.10	1392	7	1500	31
KNO_3 (4)	619	20	0.10	1177	2.58	1383	8	1557	19
$CsNO_3$ (1)	639	31	0.14	1233	0.59	1280	8	1377	54
$CsNO_3$ (2)	649	54	0.25	1253	0.59	1318	11	1389	69
$CsNO_3$ (3)	664	55	0.25	1288	0.97	1414	13	1463	63
$CsNO_3$ (4)	657	39	0.18	1273	0.59	1338	11	1443	71
$NaNO_3$ (1)	618	53	0.08	1173	0.99	1322	15	1565	88
$NaNO_3$ (2)	617	39	0.06	1170	0.98	1376	21	1535	75
$NaNO_3$ (3)	635	52	0.08	1220	0.53	1304	16	1542	68
$NaNO_3$ (4)	657	62	0.09	1279	0.61	1426	24	1540	58

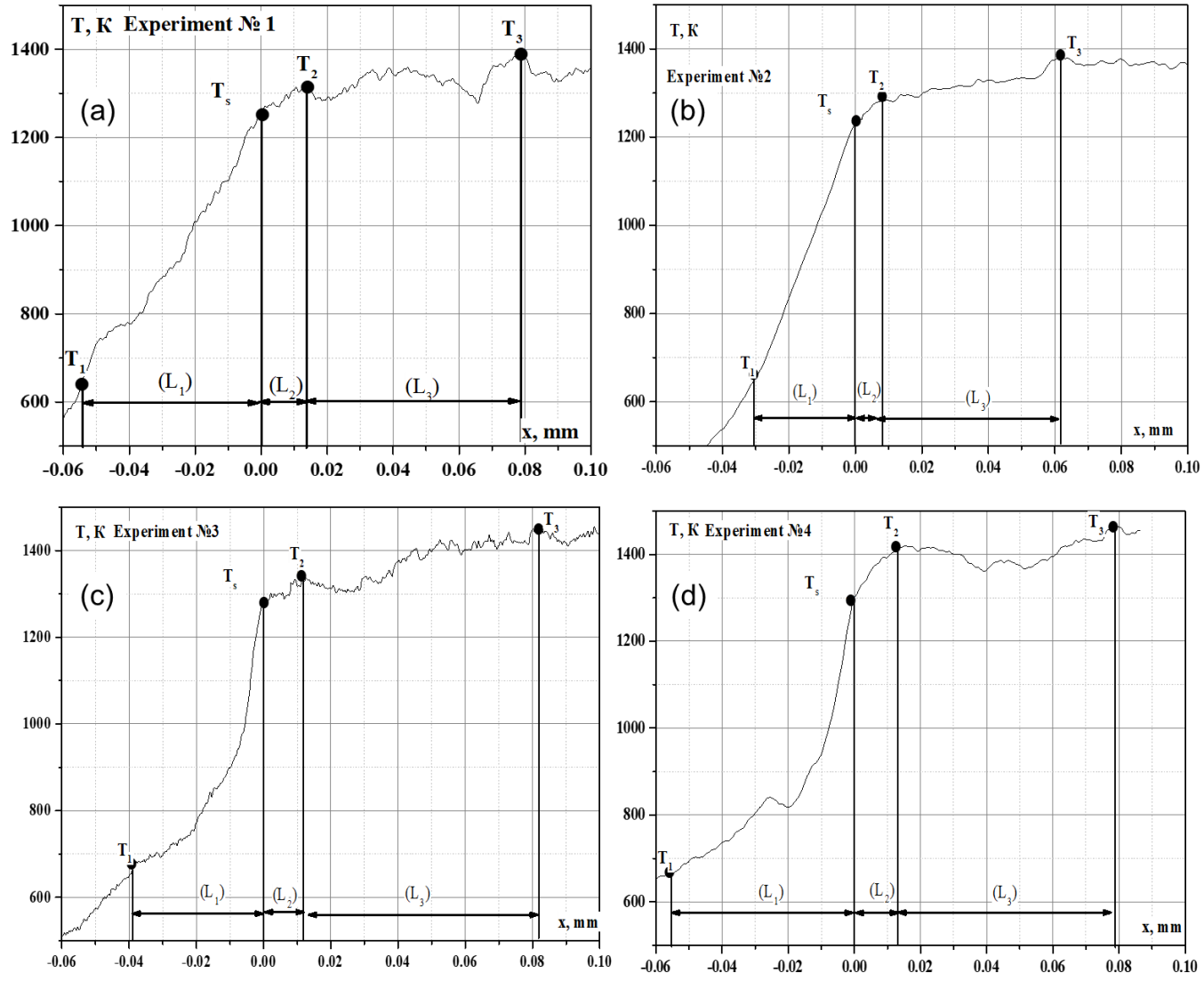

Fig. 6. The typical oscillogram of the temperature profiles in the combustion wave of the $CsNO_3$-based sample at atmospheric pressure

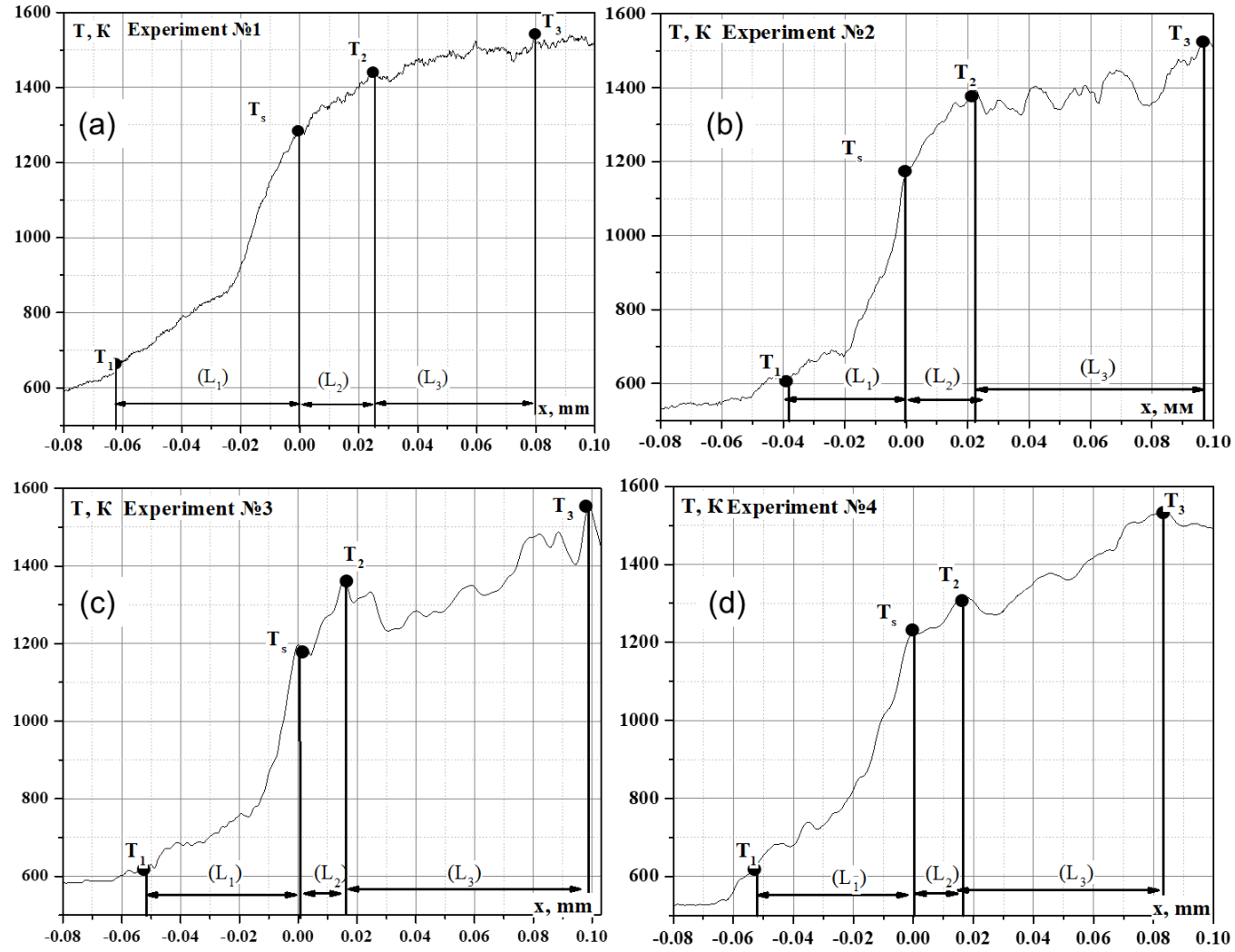

Fig. 7. The typical oscillogram of the temperature profiles in the combustion wave of the $NaNO_3$-based sample at atmospheric pressure

For the $NaNO_3$-based sample, the temperature parameters are specified as follows: Ts values ranging from 1170 to 1279 K (**Table 1, Fig.** 7); thermal diffusivity χ approximately between 0.06 and 0.09 mm^2/s; temperature gradient over the combustion surface ranging from 0.53 to 0.99×10^4 K/mm; and the value of T_1 within the range of 617 to 653 K.

The obtained results clearly demonstrated that all oscillograms exhibited a qualitatively identical pattern for the fast-burning KNO_3-based sample: Three distinct combustion zones were clearly visible, and the combustion wave parameters in parallel experiments closely aligned. A notable feature was the high value of T_s (average T_s~1264 K), a large gradient (1.98×10^4 K/cm), and a very narrow g-phase width (31 μm) (**Table 2**). These parameters are comparable to those of a similar composition with KNO_3 (α~0.88) [20]: the burning rate of this sample was 3.1 mm/s, T_s was 1305 K, the length of the g-phase was 27 μm, and $\phi=2.1 \times 10^4$ K/mm.

The temperature profiles within the combustion wave of the fast-burning $CsNO_3$-based and slow-burning $NaNO_3$-based samples exhibited no qualitative difference from that of the KNO_3-based composition (**Table 2**). All samples exhibited a high surface temperature, T_s, ranging from 1210 K to 1264 K. The $NaNO_3$-based sample showed the lowest T_s value (1210 K), whereas the $CsNO_3$-based sample exhibited T_s (1262 K), approximately equal to the KNO_3-based sample. Notably, the burning rate of the $NaNO_3$-based sample was 3.1-3.5 times lower than that of the $CsNO_3$ and KNO_3-based samples.

For the studied samples, the width L_2 ranges from 8 to 19 μm, corresponding to the zone where g-phase reactions between the decomposition products of the plasticizer and oxygen are completed, and microscopic soot particles burn out. The experimental combustion temperature for all samples is close to the calculated (T_t). The presence of condensed-phase species during combustion can disrupt the temperature profiles, leading to inaccuracies in the measurement process. Experimental findings indicate that the deviation in measured temperature values lies within the range of 3 to 5%, and the temperature deviation remains small (<1%).

Table 2. Mean values of temperature profile parameters within the combustion wave of samples

Sample-based on	T_1 (K)	L_1 (μm)	χ (mm^2/s)	T_s (K)	ϕ (10^{-4} K/mm)	T_2 (K)	L_2 (μm)	T_3 (K)	L_3 (μm)	T_1 (K)	L_1 (μm)
	+21	+6	+0.04	+63	+0.6	+37	+2	+25	+8		
KNO_3	652	18	0.09	1264	1.98	1407	8	1535	23	5.2	1516
	-33	-8	-0.04	-87	-0.81	-24	-5	-35	-4		
	+12	+9	+0.04	+26	+0.29	+76	+2	+45	+7		
$CsNO_3$	652	45	0.21	1262	0.68	1338	11	1418	64	4.6	1378
	-13	-14	-0.07	-29	-0.09	-58	-3	-41	-10		
	+25	+10	+0.01	+69	+0.21	+69	+5	+19	+16		
$NaNO_3$	632	52	0.08	1210	0.78	1357	19	1546	72	1.5	1585
	-15	-13	-0.02	-40	-0.25	-53	-4	-11	-14		

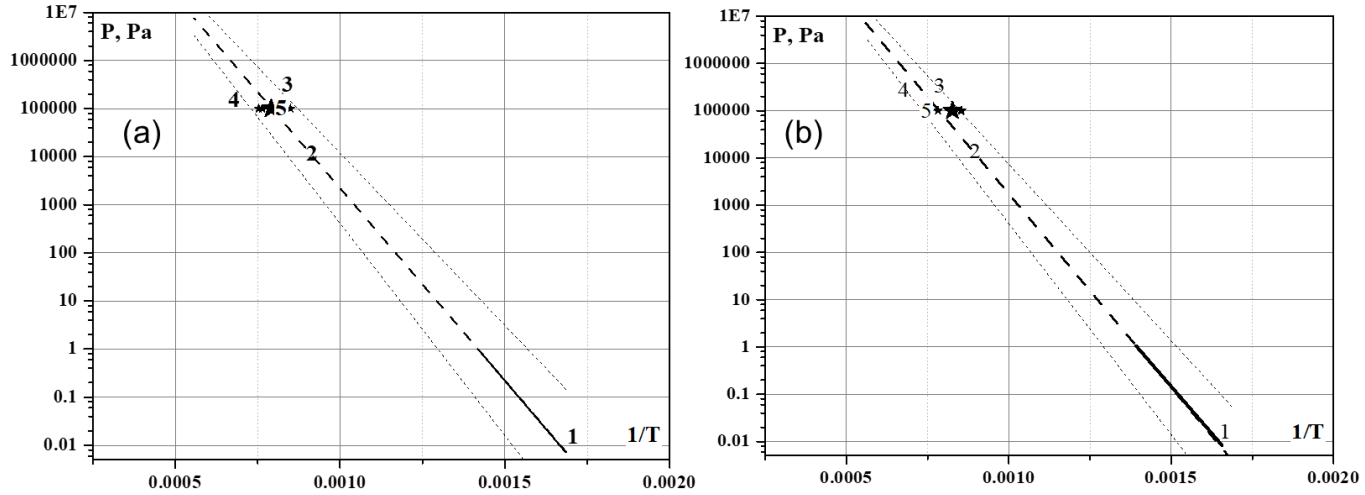

Fig. 8. Dependence of the vapor pressure of KNO_3 (a) and $NaNO_3$ (b) on temperature (solid line 1), approximation of the dependence to the high-temperature region (thick dashed line 2), and the temperature surface of the samples at a pressure of 0.1 MPa (points 5). The thin dotted line shows the error intervals at vapor pressure (lines 3 and 4)

Based on the experimental combustion temperature profile, the value of T_1 of the studied samples (632-652K) was approximately equal to the flash point of the samples determined from the TGA curves. The dependence of the vapor pressure of KNO_3 and $NaNO_3$ on temperature (up to 722 K) has been previously investigated [24]: for KNO_3:

$$log\ p(KNO_3, Pa) = (-7994 \pm 830)/T + (11.34 \pm 0.10)$$

for $NaNO_3$:

$$log\ p(NaNO_3, Pa) = (-8200 \pm 730)/T + (11.44 \pm 0.10)$$

Using the extrapolation method and the above equations, the boiling points of KNO_3 and $NaNO_3$ at atmospheric pressure were 1263 ± 151 K and 1276 ± 133 K, respectively (**Fig. 8**). The interpolated results showed good agreement with experimental observations of KNO_3 vaporization behaviour. According to the previous literature, the decomposition of KNO_3 occurs in two partially overlapping stages at temperatures above 773 K, with complete decomposition (accompanied by the vaporization of K_2O) -only occurring above 1273 K [1, 3]. Similarly, $NaNO_3$ begins to decompose slowly at approximately 873 K, accelerates above 1023 K, and completes at 1183 K under a heating rate of 15 K/min [5-7, 10]. Considering the experimental errors of all measurements, the boiling points - the points of complete decomposition of nitrates (with peaks of M^+, MNO_2^-, MNO_3^+, NO, N_2O, N_2 when M = Na, K) are close to the surface temperatures in the combustion wave of the KNO_3-based (1264 K) and $NaNO_3$-based (1210 K) samples.

3.3. Heat Balance of Combustion in c-phase

According to the parameters obtained in the combustion wave, the heat balance was calculated as Equation (9).

$$C_p(T_s - T_0) + \Delta H_{melt.} + \Delta H_v + \Delta H_{transition} = Q_c + Q_\lambda \quad (9)$$

Where T_s is combustion surface temperature (K); T_0 is initial temperature (K); C_p is the average heat capacity of the sample in the temperature range from T_s to 293 K [5-7, 9, 25-32]; ΔH_{melt} is melting enthalpy, which ΔH_{melt} for PFR [29, 30], KNO_3, $CsNO_3$, and $NaNO_3$ is 66, 96.9, 70.8, 177.5 J/g, respectively; ΔH_v is enthalpy of vaporization, which ΔH_v for DBP [30] is 289.5 J/g; $\Delta H_{transition}$ is enthalpy of polymorphic transitions of component, which $\Delta H_{transition}$ for KNO_3, $CsNO_3$, and $NaNO_3$ is 5.04, 3.6, and 3.4 kJ/mol

Table 3. Heat balance in the c-phase

Sample-based on	C_p ($J.g^{-1}.K^{-1}$)	λ ($J.K^{-1}.cm^{-1}.s^{-1}$)	T_s (K)	ΣQ ($J.g^{-1}$)	Q_λ ($J.g^{-1}$)	Q_c ($J.g^{-1}$)	$Q_c/\Sigma Q$ (%)	$Q_{c.f.}$ ($J.cm^{-2}.s^{-1}$)
				+90	+73	+198	+7	
KNO_3	1.45	0.00116	1264	1552	239	1312	84	1207
				-127	-98	-189	-6	
				+23	+18	+16	+1	
$CsNO_3$	0.82	0.00087	1262	947	44	903	95	1092
				-25	-6	-19	-1	
				+115	+100	+196	+7	
$NaNO_3$	1.70	0.00132	1210	1800	363	1433	79	401
				-75	-118	-166	-6	

[24-29], respectively; Q_c is the heat released in the c-phase (J/g); $Q_\lambda=\lambda\phi/\rho r_b$ is the heat received from the g-phase (J/g); λ is the thermal conductivity of the g-phase; r_b is the sample burning rate; ϕ is the temperature gradient in the gas zone; ρ is the density of the sample (g/cm^3), ΣQ is the sum of the terms on the left side of the equation (J/g); $Q_c/\Sigma Q$ is the relative share of heat released in the c-phase (%).

The data presented in **Table 3** highlight the variations in the released heat within the reaction layer of the c-phase, as well as the overall heat amount ($\sum Q=Q_c+Q_\lambda$) for the examined samples. The burning rate is dictated by the heat transferred per unit time from the reaction zone in the c-phase to generate the next heated layer (Equation 10).

$$Q_{c.f.} = Q_c.r_b.\rho \text{ J/(cm}^2\text{.s)}. \quad (10)$$

The KNO_3-based sample exhibited the highest flux value $Q_{c.f.}$ (1207 $J/(cm^2.s)$). The $NaNO_3$-based sample exhibited the smallest value (401 $J/(cm^2.s)$), approximately 3 times less than that of the KNO_3-based sample. Accordingly, the samples can be arranged in the following order based on $Q_{c.f.}$ values: $K^+ > Cs^+ > Na^+$ (consistent with their burning rates).

The main amount of heat, which is necessary for combustion propagation of the studied samples, was released in the reaction layer of the c-phase ($Q_c/\Sigma Q \geq 79\%$).

CONCLUSION

This study evaluated the burning surface temperature and heat release behavior of nitrate-containing energetic formulations based on KNO_3, $CsNO_3$, and $NaNO_3$. Thermogravimetric analysis (TGA) determined the flash points in the range of 653 - 683 K for the studied samples. Combustion proceeds predominantly in two zones -condensed (c) phase and gas (g) phase - each of which comprises several functional regions: preheating, initial decomposition, main exothermic reaction (driven by interactions between binder decomposition products and nitrogen oxides/O_2), and one region associated with bigger particle reactions.

All samples exhibited high surface temperatures under atmospheric conditions (T_s > 1200 K). The characteristic parameter T_1, defined as the depth at which the surface temperature decreases by a factor of *e*, correlated closely with the TGA-derived ignition thresholds to verify combustion layer dynamics. Combustion propagation was primarily driven by reactions in the condensed phase, which accounted for 79-95% of the total heat release. Among all the tested formulations, the KNO_3-based sample produced the highest surface heat-flow density.

These findings provide a detailed phase-based understanding of combustion behavior in nitrate-based energetic materials and emphasize the dominant role of condensed-phase reactions. The established correlation between T_1 and TGA-based flash points offers a practical diagnostic for predicting ignition behavior in related formulations. These insights are critical for the development of thermally stable, high-efficiency pyrotechnic and propellant systems.

SUPPORTING INFORMATION

This article contains no supporting material.

ACKNOWLEDGEMENTS

This research did not receive any specific funding. All authors expresses sincere gratitude to all parties who have supported us.

CONFLICT OF INTEREST

The authors declare that they have no known competing financial interests or personal relationships that could have influenced the work reported in this paper.

AUTHOR CONTRIBUTIONS

Nguyen Duy Tuan: Methodology, Investigation, Data analysis, Writing manuscript, Manuscript editing and discussion. Denisuyk A.P.: Data analysis, Supervision, Writing manuscript. Hoang Trung Huu: Writing manuscript. Doan Minh Khai: Data analysis, Manuscript editing and discussion. Sizov V.A.: Data analysis.

REFERENCES

[1] Freeman E.S. 1957. The kinetics of the thermal decomposition of potassium nitrate and of the reaction between potassium nitrite and oxygen[1a]. *J. Am. Chem. Soc.* 79. 838-842.

[2] Turcotte R., Fouchard R., Turcotte A.-M., Jones D. 2003. Thermal analysis of black powder. *J. Therm. Anal. Calorim.* 73. 105-118. doi: 10.1023/A:1025181424038

[3] Pouretedal H.R., Ebadpour R. 2014. Application of non-isothermal thermogravimetric method to interpret the decomposition kinetics of $NaNO_3$, KNO_3, and $KClO_4$. *Int. J. Thermophys.* 35(5). 942-951. doi: 10.1007/s10765-014-1636-y

[4] Hosseini, S. and Eslami, A. 2010. Thermoanalytical investigation of relative reactivity of some nitrate oxidants in tin-fueled pyrotechnic systems. *J. Therm. Anal. Calorim.* 101(3). 1111-1119. doi: 10.1007/s10973-010-0813-x

[5] Gordon, S. and Campbell, C. 1955. Differential thermal analysis of inorganic compounds. *Anal. Chem.* 27(7). 1102-1109.

[6] Stern, K.H. 1972. High temperature properties and decomposition of inorganic salts part 3, nitrates and nitrites. *J. Phys. Chem. Ref. Data.* 1(3). 747-772. doi: 10.1063/1.3253104

[7] Mohammad, M.B., Brooks, G.A. and Rhamdhani, M.A. 2018. Premelting, melting, and degradation properties of molten alkali nitrates: $LiNO_3$, $NaNO_3$, KNO_3, and binary $NaNO_3$-KNO_3. *Metall. Mater. Trans. B.* 49(3). 1482-1498. doi: 10.1007/s11663-018-1205-z

[8] Bond, B.D. and Jacobs, P.W.M. 1966. The thermal decomposition of sodium nitrate. *J. Chem. Soc. A.* 1265-1268. doi: 10.1039/J19660001265

[9] Kouassi, E.K., Manouan, M.W., Zoro, E., Boa, D., Benigni, P., Zamali, H., Rogez, J. and Hellali, D. 2021. Experimental investigation and thermodynamic evaluation of the $CsNO_3$-$LiNO_3$-$NaNO_3$ ternary system. *J. Alloys Compd.* 864. 158131. doi: 10.1016/j.jallcom.2020.158131

[10] Freeman, E.S. 1956. The kinetics of the thermal decomposition of sodium nitrate and of the reaction between sodium nitrite and oxygen. *J. Phys. Chem.* 60(11). 1487-1493.

[11] Singh, H. and Bhaskara Rao, R., 1990. Temperature sensitivity of magnesiu - sodium nitrate propellants. *Prop., Explos., Pyrotech.* 15(6). 250-253. doi: 10.1002/prep.19900150605

[12] Singh, H. and Bhaskara Rao, R. 1992. Effect of particle size on combustion of magnesium-sodium nitrate propellants. *Combust. Sci. Technol.* 81(4-6). 233-242. doi: 10.1080/00102209208951804

[13] Silin, N.A., Kashporov, L.Y., Sheludyak, Y.E., Asmatullov, Z.E., Raspopin, A.G. and Grineeva, R.A. 1992. Combustion rate functional dependence on various variables for the Mg+ $NaNO_3$ mixture. *Combust. Explos. Shock Waves.* 28(5). 474-481. doi: 10.1007/BF00755717

[14] Singh, H., Somayajulu, M.R. and Rao, R.B. 1989. A study on combustion behavior of magnesium · sodium nitrate binary mixtures. *Combust. Flame.* 76(1). 57-61. doi: 10.1016/0010-2180(89)90077-1

[15] Guo, Z., Guan, H., Shi, C. and Zhou, B. 2024. Study of combustion characteristics of Magnesium/Strontium Nitrate and Magnesium/Sodium Nitrate pyrotechnics under low pressure environment. *Combust. Sci. Technol.* 196(15). 3365-3381. doi: 10.1080/00102202.2023.2175608

[16] Pouretedal, H.R. and Ravanbod, M. 2015. Kinetic study of ignition of Mg/$NaNO_3$ pyrotechnic using non-isothermal TG/DSC technique. *J. Therm. Anal. Calorim.* 119(3). 2281-2288. doi: 10.1007/s10973-014-4330-1

[17] Denisyuk, A.P., Duy Tuan, N. and Sizov, V.A. 2022. Combustion behavior of the inorganic nitrates - based compositions. part ii: effect of Al and Al - Mg alloy on burning rate. *Prop., Explos., Pyrotech.* 47(5). e202100145. doi: 10.1002/prep.202100145

[18] Denisyuk, A.P., Duy Tuan, N. and Sizov, V.A. 2020. Combustion behavior of the inorganic nitrates - based compositions part I. *Prop., Explos., Pyrotech.* 45(9). 1382-1387. doi: 10.1002/prep.202000053

[19] Tuan, N.D., Denisuyk, A.P., Khai, D.M. and Sizov, V.A., 2023. Influence of some additives on burning rate of KNO_3-based compositions. *Vietnam J. Sci. Technol.* 61(6). 1000-1009. doi: 10.15625/2525-2518/17077

[20] Denisyuk, A., Rusin, D. and Long, N. 2007. Mechanism of combustion of fire-extinguishing propellants based on potassium nitrate. *Dokl. Phys. Chem.* 414(1). 99. doi: 10.1134/S0012501607050016

[21] Jiang, H., Wang, J., Wu, S., Yuan, Z., Hu, Z., Wu, R. and Liu, Q. 2012. The pyrolysis mechanism of phenol formaldehyde resin. *Polym. Degrad. Stab.* 97(8). 1527-1533. doi: 10.1016/j.polymdegradstab.2012.04.016

[22] Shtessel', E.A. and Dorozhevets, I.N. 1990. Combustion of heterogeneous condensed systems in the presence of chemical transport reactions. *Combust. Explos. Shock Waves.* 26(1). 52-59. doi: 10.1007/BF00742272

[23] Bakhman, N.N. and Belyaev, A.F. 1967. *Combustion of heterogeneous condensed systems* (No. RPETRANS19). https://apps.dtic.mil/sti/html/tr/AD0670440/

[24] Dukhanin, G.P. and Lopatin, S.I. 2011. Mass-spectrometric examination of vaporization of sodium nitrite and sodium and potassium nitrates. *Russ. J. Appl. Chem.* 84(2). 184-189. doi: 10.1134/S1070427211020030

[25] Ichikawa, K. and Matsumoto, T. 1983. The heat capacities of lithium, sodium, potassium, rubidium, and caesium nitrates in the solid and liquid states. *Bull. Chem. Soc. Jpn.* 56(7). 2093-2100.

[26] Maeso, M.J. and Largo, J. 1993. The heat capacities of $LiNO_3$ and $CsNO_3$ from 350 to 700 K. *Thermochim. Acta.* 222(2). 195-201. doi: 10.1016/0040-6031(93)80552-L

[27] Jriri, T., Rogez, J., Bergman, C. and Mathieu, J.C. 1995. Thermodynamic study of the condensed phases of NaNO3, KNO3 and $CsNO_3$ and their transitions. *Thermochim. Acta.* 266. 147-161. doi: 10.1016/0040-6031(95)02337-2

[28] Korabel'nikov, D.V. and Zhuravlev, Y.N. 2013. Theoretical study of the thermodynamic properties of lithium, sodium, and potassium nitrates. *Phys. Solid State.* 55(8). 1765-1772.2. doi: 10.1134/S1063783413080155

[29] Takahashi, Y., Sakamoto, R. and Kamimoto, M., 1988. Heat capacities and latent heats of $LiNO_3$, $NaNO_3$, and KNO_3. *Int. J. Thermophys.* 9(6). 1081-1090. doi: 10.1007/BF01133275

[30] Deshpande, V.V., Karkhanavala, M.D. and Rao, U.R.K., 1974. Phase transitions in potassium nitrate. *J. Therm. Anal. Calorim.* 6(6). 613-621. doi: 10.1007/bf01911781

[31] Wypych, G., 2004. *Handbook of plasticizers*. ChemTec Publishing.

[32] Godwin, A.D., 2024. *Plasticizers*. In Applied plastics engineering handbook (pp. 595-618). William Andrew Publishing. Doi: 10.1016/B978-0-323-88667-3.00031-X